Geophysical Journal International

Geophys. J. Int. (2011) **187,** 1319–1333 doi: 10.1111/j.1365-246X.2011.05245.x

The rotational stability of a convecting earth: assessing inferences of rapid TPW in the late cretaceous

N.-H. Chan,[1] J.X. Mitrovica,[1] I. Matsuyama,[2] J.R. Creveling[1] and S. Stanley[3]

[1] *Department of Earth & Planetary Sciences, Harvard University, 20 Oxford Street, Cambridge,* MA 02138, *USA. E-mail: nhchan@eps.harvard.edu*
[2] *Department of Earth & Planetary Science, University of California, 307 McCone Hall, Berkeley,* CA 94720, *USA*
[3] *Department of Physics, University of Toronto,* 60 *St. George Street, Toronto,* ON M5S 1A7, *Canada*

Accepted 2011 September 22. Received 2011 July 12; in original form 2011 March 25

SUMMARY

We outline a linearized rotational stability theory for predicting the time dependence of true polar wander (TPW) on a Maxwell viscoelastic body in response to mantle convective loading. The new theory is based on recent advances in ice age rotation theory. A comparison between predictions based on the new theory and analytic expressions for equilibrium (infinite-time) TPW on planetary models with elastic lithospheres demonstrates that the linearized theory can, in the case of loading at mid-latitudes, predict TPW of over 20° to better than 5 per cent accuracy. We present predictions of TPW for loading with periodic and net ramp-up time histories. Moreover, we compare the time dependence of TPW under assumptions consistent with the canonical equilibrium stability theory adopted in most previous analyses of convection-induced TPW, and a stability theory that includes two effects that have not been considered in previous geophysical analyses: (1) the so-called 'remnant rotational bulge' associated with the imperfect reorientation of the rotational bulge due to the presence of an elastic lithosphere; and (2) a stable (over the timescale of the forcing) excess ellipticity. As a first application of the new theory, we consider recent inferences of rapid (order 1 Myr) TPW motion of amplitude 10°–20° during the Late Cretaceous. We conclude that excursions of this amplitude and timescale are physically implausible.

Key words: Earth rotation variations; Palaeomagnetic secular variation; Rheology: crust and lithosphere.

1 INTRODUCTION

The stability of the Earth's rotation vector in response to thermal convective motions in the mantle has been, and remains, the subject of active debate within the geophysical and geological literature. In general, predictions of the convection-induced reorientation of the rotation vector relative to the surface geography, or true polar wander (henceforth TPW) (e.g. Steinberger & O'Connell 1997) have been based on a canonical equilibrium stability theory outlined by Gold (1955), and summarized, schematically, in Fig. 1. Consider an Earth model in steady rotation for a time long enough that all viscous stresses have relaxed to the imposed centrifugal potential (Fig. 1A1); in this case, the equilibrium 'rotational bulge' or ellipticity of the planet will have a so-called hydrostatic form (Nakiboglu 1982). If the Earth is then subject to a positive load, polar motion would act to move the load toward the equator (Fig. 1A2); the background bulge of the planet will initially resist such an excursion. However, the Earth will deform in response to the perturbed centrifugal potential, and the bulge will eventually reorient perfectly to the new rotation vector (Fig. 1A3); this will free the pole to wander further from the load (Fig. 1A4). The process will continue in infinitesimal steps until the load has migrated to the equator (Fig. 1A5) and TPW will cease. In this theory, the rotation vector is ultimately unstable in the presence of an applied load since the bulge does not provide any long-term resistance to TPW (Gold 1955; Goldreich & Toomre 1969). The Earth, in this scenario, is said to have no permanent memory of its orientation. (Note that there is an assumption in this classic description that the applied load will never reach a state of isostatic compensation, and will thus continuously act as a driving force on the pole.)

The physical basis for this description of rotational stability has been highlighted by two equally canonical schematic images. For example, the continual effort by the bulge to keep up with the rotation pole is illustrated by Gold's famous donkey and carrot analogy, whereby a donkey (representing the bulge) moves inexorably toward a carrot (the pole) that is connected to the donkey by an overhead wire that dangles frustratingly in his line of sight (Gold 1955). A key element of the Gold stability theory is that any load, no matter what size, will drive a TPW that eventually moves the load to the equator. This key aspect of the theory was discussed by Goldreich & Toomre (1969), who characterized the load by a small beetle, or a set of such beetles. It is important to emphasize that the 'equilibrium'

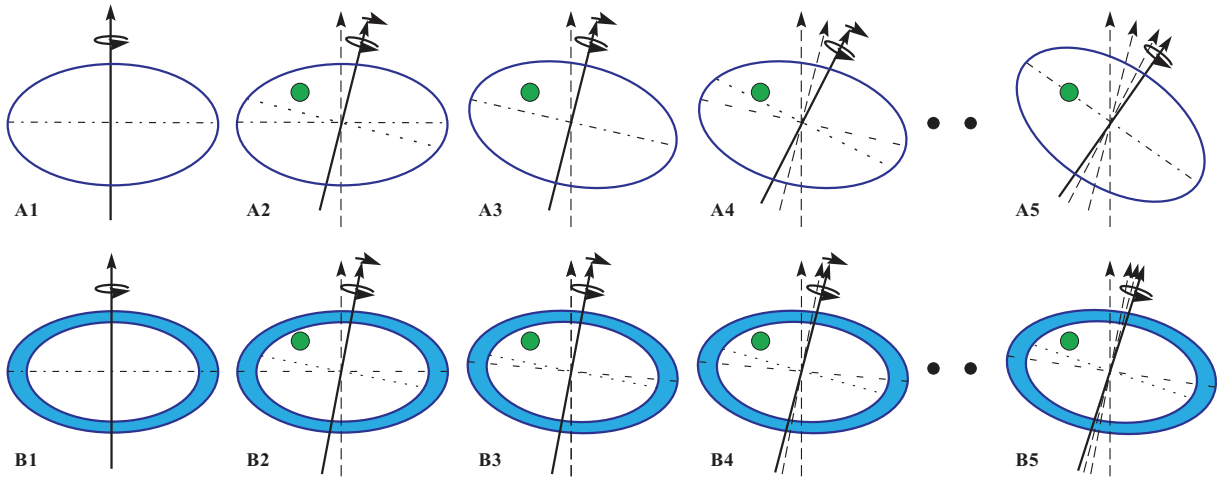

Figure 1. Schematic illustration of the physics of TPW as treated by (A) (Gold 1955) and (B) Willemann (1984) and Matsuyama *et al.* (2006). The green disk represents a positive internal density load, the blue outer shell (second row) is an elastic lithosphere, the solid arrow (with spin and TPW directions specified at the head and tip, respectively) is the rotation vector, and the long-dashed arrows are previous rotation vectors within the same series. On each frame, a dashed line denotes the plane of the rotational bulge, while the dotted line is the rotational equator. When these two lines are aligned (A1, A3, A5, B1), the bulge is perfectly relaxed. (A) TPW on an Earth model in which the rotational bulge will ultimately adjust completely to load-induced TPW, and the load will ultimately migrate to the equator (A5). (B) TPW when an initial, hydrostatic form (B1) includes an unstressed elastic lithosphere. In this case, the elastic shell will permanently resist excursions of the rotation pole and the final state (B5), in which the load has not reached the equator, will represent a balance between this resistance and the load-induced impact on the pole.

stability theory of Gold yields a prediction of the final orientation of the pole and says nothing about the timescale required to reach the equilibrium position.

In mathematical terms, the orientation of the rotation pole in the Gold stability theory is given by the direction of the principal axis of the non-hydrostatic inertia tensor. In this regard, under the assumption that the timescale of convection is much longer than the timescale of bulge adjustment, the TPW path in convection studies has generally been computed by diagonalizing the inertia tensor perturbation at each step in the simulation (Steinberger & O'Connell 1997). This perturbation takes into account the advection of density heterogeneities and deformation of all boundaries associated with the mantle flow.

A small number of studies have extended the rotational stability theory described above to consider the time history of TPW (e.g. Ricard *et al.* 1993; Richards *et al.* 1997, 1999; Tsai & Stevenson 2007; Schaber *et al.* 2009). Tsai & Stevenson (2007), for example, used scaling arguments based on energy considerations to derive analytic expressions for the TPW of a Maxwell body with a single relaxation time. Their study highlights several important concepts that will also be apparent in the results we describe within this paper. For example, a central goal of their analysis was to quantify the 'speed limit' of TPW—how fast can the pole go in response to convective forcing? In this regard, it is important to point out that there is, of course, no minimum speed—a load the size of the beetle may eventually get to the equator using the theory of Gold (1955), but it may take longer than the age of the Earth to do it. Tsai & Stevenson (2007) also introduced the concept of a TPW filter. In particular, they argued that TPW will most efficiently be excited by the longest timescales of the forcing, and the transition or cut-off within this low (frequency) pass filter will be governed, in large part, by the mantle viscosity. Fig. 1 in Tsai & Stevenson (2007) is a particularly elegant demonstration of this physics.

Tsai & Stevenson (2007) used their model to conclude that the maximum TPW rate is 2.4°Myr^{-1}, though they emphasize that this rate is sustainable for only a short period of time. They concluded that this rate appears to be too high relative to the geological record, at least in the post-Jurassic period, and they provided a suite of possible explanations for this discrepancy (see p. 9 of their paper). One of these explanations is that the lower mantle viscosity may be higher than they considered; an increase in this viscosity would act to slow the convective driving force for TPW. An earlier convective simulation of polar motion over the last 100 Myr (Steinberger & O'Connell 1997), based on the rotational stability theory of Gold (1955), also required a high deep mantle viscosity to achieve TPW rates consistent with palaeomagnetic data. Tsai & Stevenson (2007) also noted that their TPW speed limit was too low to allow the 90° shift in ∼40 Myr inferred for the early Cambrian by Kirschvink *et al.* (1997). They concluded that the polar motion postulated by Kirschvink *et al.* (1997) was dynamically implausible.

Tsai & Stevenson (2007) did not include the possible stabilizing effect of an elastic, or even high-viscosity viscoelastic lithosphere. They suggested that broken plates do not provide any resistance to changes in the centrifugal potential (since adjustments would, they argued, be taken up along plate boundaries), and that the timescale associated with the elastic adjustment of the lithosphere would be short relative to the characteristic timescale of the convective forcing. In regard to the first argument, the centrifugal force will act within the entire body of the planet, and will therefore cause flexure, and resistance to TPW, throughout the plate—not only at plate boundaries. It is certainly true that the effective elastic thickness of a broken plate in response to a body force with a spherical harmonic degree two potential (i.e. the centrifugal force) will be smaller than the elastic thickness of an unbroken shell, but it will not be zero. This will be particularly true in considering TPW over timescales of order several Myr or less; for instance, modelling of ice age adjustments clearly requires the incorporation of a strong lithosphere (e.g. Nakada & Lambeck 1989). In regard to the second argument, while the elastic response of the lithosphere will certainly have a timescale that is short relative to the convective forcing, the presence of such a lithosphere—even a broken one—will nonetheless have a potentially profound impact on rotational stability. This impact

is illustrated in Fig. 1(B), which extends the stability arguments in Fig. 1(A) (Gold 1955) to include an elastic lithospheric shell.

The equilibrium rotational stability of dynamic, terrestrial planets with elastic lithospheres was first treated by Willemann (1984), and most recently by Matsuyama *et al.* (2006) and Daradich *et al.* (2008), who corrected minor errors in the original description. Consider the model planet in Fig. 1(B1), which is characterized by a hydrostatic background oblateness (i.e. the flattening in Fig. 1B1 is identical to that in Fig. 1A1). Let us assume the planet has an unstressed elastic lithosphere, as denoted by the light blue shell. An unstressed shell may have developed, for example, through secular cooling of the planet, or by very slow viscous relaxation within the lithosphere. If this planet is subsequently loaded (Fig. 1B2), the pole would (as in Fig. 1A2) move away from the load and the bulge will resist this motion. However, the important distinction between this case and Fig. 1(A) is that the adjustment of the bulge in response to TPW cannot perfectly reorient the bulge (i.e. the elastic shell cannot deform to be symmetric about the new pole position; Fig. 1B3). The deviation from scenario 1A arises because elastic stresses that develop in the (initially unstressed) lithosphere in response to the perturbed centrifugal potential will impose a permanent restoring force on the rotation vector. That is, in this case, the system will have a memory of its initial state, and the ultimate result is that the final equilibrium pole position (Fig. 1B5) will reflect a balance between loading and what Willemann (1984) and Matsuyama *et al.* (2006) called the 'remnant rotational bulge'. Most notably, TPW will cease before the load makes it to the equator.

The stabilization associated with the lithosphere is significant. As an example, taken from the results of Matsuyama *et al.* (2006), consider a load with a pre-compensated size that is 10 per cent of the size of the equatorial bulge, where 'size' is measured by the associated geopotential perturbation at spherical harmonic degree two. If this load is placed at a colatitude of 40°, then the Gold (1955) theory predicts a total TPW of 50° (since the load will ultimately reach the equator). In contrast, if a lithosphere of thickness of 50 km is assumed, then the extended equilibrium stability theory summarized in Fig. 1(B) ultimately yields a TPW of only 4°. Two caveats. First, if the 50 km lithosphere is broken, then the effective elastic thickness will be smaller than this value, but it will not be zero; it is important, in this regard, to note that the stabilization associated with the remnant rotational bulge is relatively insensitive to the adopted lithospheric thickness (Willemann 1984; Matsuyama *et al.* 2006). For example, if we repeat the calculation for an elastic lithospheric thickness of 25 km, the total TPW predicted by Matsuyama *et al.* (2006) would still be less than 5°. Secondly, if the lithosphere were treated as viscoelastic rather than elastic, then the stabilization associated with the remnant bulge would not be permanent. Rather, it would only stabilize the rotation pole in response to forcings with timescales less than the relaxation time of the high viscosity lithosphere. In this regard, it would act, as in the terminology of Tsai & Stevenson (2007), as a low pass TPW filter. In any event, the rather dramatic damping of TPW associated with the presence of an elastic or high viscosity lithosphere suggests that the remnant bulge physics should be incorporated into the rotational stability theory.

In this paper, we outline a linearized stability theory for the rotation of Earth models with a 1-D (depth varying) linear viscoelastic rheology. The theory extends the approach described by Tsai & Stevenson (2007) in a number of ways. First, it admits as many relaxation times (or normal modes) as exist in the impulse response of the Earth model. Secondly, the 1-D depth variation accommodates an elastic or finite viscosity lithosphere, and thus incorporates the possibility of stabilization from the remnant rotational bulge. The theory also allows for the possibility of an excess ellipticity in the Earth's form which might arise from a number of processes acting on timescales much longer than the convective flow considered in this manuscript (see below). The theory is based on a linearized version of the time domain Euler equation, and it follows recent developments in the theoretical treatment of ice age Earth rotation (Mitrovica *et al.* 2005). The linearization assumes 'small' motions of the rotation pole; however, we present results that indicate that the TPW can reach 20°–30° (or 40°–60° motion centred on the original pole position) before errors exceed order 5–10 per cent. And thus, within this range of TPW we explore the full complexity of the time dependence of the TPW.

To investigate the time dependence of TPW, we need to specify a time history of the convective forcing (i.e. a time history of perturbations to the inertia tensor). Tsai & Stevenson (2007) considered sinusoidal variations in the TPW forcing, in contrast to earlier studies that tended to explore rotational stability in response to a step-wise change in the inertia tensor (e.g. Munk & MacDonald 1960). The time variation in the inertia tensor driven by mantle flow almost certainly includes both classes of forcing—indeed, Goldreich & Toomre (1969) demonstrated that the timescale for inertia tensor changes can be short if there are multiple contributors to the forcing—and thus our analysis will consider both a sinusoidal time history and a history involving a gradual ramp-up or net shift in the load.

As a first application of our theory, we will investigate the plausibility, from the perspective of rotational dynamics, of evidence for a rapid TPW event in the Late Cretaceous (Sager & Koppers 2000). Specifically, Sager & Koppers (2000) inferred 16°–21° of TPW in 2–5 Myr beginning at ∼85 Ma on the basis of palaeomagnetic data from Pacific seamounts. More recently, there has also been a preliminary suggestion, based on magnetostratigraphic data, of rapid (order 1 Myr), quasi-cyclical 10°–20° TPW during the Late Cretaceous (Thissen *et al.* 2010). With the expectation that such high resolution analyses will become more common, the overarching goal of our study will be to establish bounds on the amplitude of TPW and elucidate the physics controlling rapid motions of the rotation pole—whether these motions are quasi-cyclical or unidirectional. The linearized theory we develop is particularly well suited to such problems, since the net polar wander during such events is well within the range of validity we establish for the linearization. Moreover, the response of the Earth to such rapid forcing is certainly characterized by some degree of elastic strength in the crust-lithosphere system, and hence the remnant bulge physics may play an important role.

We begin with a summary of the linearized theory of rotational stability.

2 A LINEARIZED THEORY OF EARTH ROTATION

In this section, we outline a linearized form of the equation governing conservation of angular momentum that is derived from recent treatments within the literature of ice age rotation (Mitrovica *et al.* 2005).

In the case where no external torques act on the system, the Euler Equation in an Earth-fixed reference frame is

$$0 = J_{ij}(t)\dot{w}_j(t) + \dot{J}_{ij}(t)w_j(t) + \epsilon_{ijk}w_j(t)J_{kl}(t)w_l(t), \qquad (1)$$

where **J** denotes the inertia tensor, w_i are components of angular velocity, ϵ_{ijk} is the Levi-Civita tensor and the dot superscript denotes a time derivative.

If we assume that the inertia tensor is diagonal in the unperturbed state, with elements given by A, A and C, and, in the same state, the angular velocity vector is given by $\mathbf{\Omega} = (0,\ 0,\ \Omega)$, then a perturbation from this initial state can be written as

$$\begin{aligned} w_i(t) &= \Omega[\delta_{i3} + m_i(t)] \\ J_{11}(t) &= A + I_{11}(t) \\ J_{22}(t) &= A + I_{22}(t) \\ J_{33}(t) &= C + I_{33}(t) \\ J_{ij}(t) &= I_{ij}(t) \ \text{ for } i \neq j, \end{aligned} \tag{2}$$

where we assume that all perturbations I_{ij} are smaller than either of the principal moments in the unperturbed system (A, C), and that $m_i \ll 1$.

There are three contributions to the inertia tensor perturbations. These are: (1) the mantle or surface mass anomalies; (2) the deformation induced by the mass anomalies, and (3) the deformation in response to the perturbed centrifugal potential. In each case, a mapping exists between the perturbation in the inertia tensor and the associated perturbation in the geopotential at spherical harmonic degree 2 (e.g. Matsuyama *et al.* 2006). We adopt a Maxwell viscoelastic rheology in the calculation of these geopotential perturbations and the latter two contributions may therefore be computed using viscoelastic Love number theory (Peltier 1974; Wu 1978; Tromp & Mitrovica 1999).

In the time (t) domain, the load and tidal (or tidal-effective) k Love numbers at spherical harmonic degree two are, respectively, given by

$$\begin{aligned} k_2^L(LT, \nu, t) &= k_2^{L,E}\delta(t) + \sum_{j=1}^{J} r_j' e^{-s_j t} \\ k_2^T(LT, \nu, t) &= k_2^{T,E}\delta(t) + \sum_{j=1}^{J} r_j'' e^{-s_j t}. \end{aligned} \tag{3}$$

The Love numbers are comprised of instantaneous elastic (first term on the right-hand side) and non-elastic (second term) components, where the latter are comprised of a set of J normal modes of viscoelastic decay. The two Love numbers share the same set of inverse decay times, s_j, but have distinct modal amplitudes. The viscoelastic Earth model structure is embedded within each of the parameters that define these Love numbers. In this regard, on the left-hand side of these equations, we make the dependence on the elastic thickness of the lithosphere, LT, and on the radial viscosity profile, ν, explicit. It will be useful to write these time domain expressions in terms of their Laplace-transform, s-domain forms. These are

$$\begin{aligned} k_2^L(LT, \nu, s) &= k_2^{L,E} + \sum_{j=1}^{J} \frac{r_j'}{s + s_j} \\ k_2^T(LT, \nu, s) &= k_2^{T,E} + \sum_{j=1}^{J} \frac{r_j''}{s + s_j}. \end{aligned} \tag{4}$$

Using eq. (2) in (1), and computing the necessary inertia tensor perturbations using the viscoelastic Love numbers, yields, after some algebra, the linearized Euler Equation (i.e. the Liouville Equation) (Mitrovica *et al.* 2005),

$$\mathbf{m}(t) = \frac{\mathbf{I}^L(t) + k_2^L(LT, \nu, t) * \mathbf{I}^L(t)}{(C - A)} + \frac{k_2^T(LT, \nu, t)}{k_f} * \mathbf{m}(t), \tag{5}$$

where $*$ denotes a time-convolution, $\mathbf{I}^L(t) = I_{13}^L(t) + i I_{23}^L(t)$, $\mathbf{m}(t) = m_1(t) + i m_2(t)$, and the observed fluid Love number, k_f, is

$$k_f = \frac{3G}{a^5\Omega^2}(C - A), \tag{6}$$

in which a and Ω are the radius and rotation rate of the Earth, and G is the universal gravitational constant.

The value of k_f governs the background oblateness of the Earth model upon which the perturbations associated with the loading are superimposed. In practise, we can separate this number into hydrostatic and non-hydrostatic (k_{nh}) contributions, where the former can be computed using viscoelastic Love number theory. Specifically, this separation can be written as

$$k_f = k_2^T(LT = 0, s = 0) + k_{nh}, \tag{7}$$

where the hydrostatic form has been replaced by the degree two k fluid Love number for a model with no elastic lithosphere at the limit of infinite time ($s = 0$); in this case, there are no purely elastic regions and all viscous regions of the model have fully relaxed—hence the dependence on ν disappears.

Applying this decomposition to eq. (5) yields

$$\begin{aligned} \mathbf{m}(t) = &\frac{\mathbf{I}^L(t) + k_2^L(LT, \nu, t) * \mathbf{I}^L(t)}{(C - A)} \\ &+ \frac{k_2^T(LT, \nu, t)}{k_2^T(LT = 0, s = 0) + k_{nh}} * \mathbf{m}(t). \end{aligned} \tag{8}$$

In the s-domain, this equation becomes

$$\mathbf{m}(s) = \frac{\mathbf{I}^L(s)}{C - A} \cdot \frac{1 + k_2^L(LT, \nu, s)}{1 - \frac{k_2^T(LT, \nu, s)}{k_2^T(LT=0, s=0) + k_{nh}}}. \tag{9}$$

We can use this last equation to revisit the physics of both scenarios shown in Fig. 1. In the rotational stability theory of Gold (1955), the background form is purely hydrostatic (i.e. $k_{nh} = 0$), and the model has no elastic lithosphere (i.e. $LT = 0$). If we furthermore assume that the load is never isostatically compensated (as Gold did), then the term in the numerator, $1 + k_2^L(LT = 0, \nu, s)$ is assumed to be non-zero in the limit of infinite time (or $s = 0$). However, in the same time limit, the denominator, $1 - k_2^T(LT, \nu, s)/[k_2^T(LT = 0, s = 0) + k_{nh}]$ will go to zero, and the linearized solution for $\mathbf{m}(s \to 0)$ becomes unbounded. Of course, in a non-linear theory, this instability continues until the load reaches the equator.

In the scenario shown in Fig. 1(B) (where we also assume $k_{nh} = 0$), the Earth model does have an elastic lithosphere. In this case, neither the numerator nor the denominator in eq. (9) will go to zero at infinite time, and the system remains stable. In this case, the final position of the load is governed by a balance between the force driving polar motion, which is proportional to the term $1 + k_2^L(LT, \nu, s)$ in the numerator, and the resistance associated with the bulge, the term $1 - k_2^T(LT, \nu, s)/k_2^T(LT = 0, s = 0)$.

It is clear from these examples that the stability of the system is ultimately governed by the ratio $k_2^T(LT, \nu, s)/[k_2^T(LT = 0, s = 0) + k_{nh}]$ that appears in the denominator of eq. (9). In the absence of a non-hydrostatic contribution to the background bulge, this means that the system will remain stable as long as $k_2^T(LT, \nu, s) \neq k_2^T(LT = 0, s = 0)$; that is, the system will remain stable as long as the Love number that governs the response of the model to the changing centrifugal potential, $k_2^T(LT, \nu, s)$, does not take on a hydrostatic form. When the lithosphere has a purely elastic component, that is, when $LT \neq 0$, this stability requirement is guaranteed, and the difference between $k_2^T(LT, s = 0)$

and $k_2^T(LT = 0, s = 0)$ represents the remnant bulge stabilization described in section 1 (Willemann 1984; Matsuyama *et al.* 2006). Note that if the Earth model has a high viscosity viscoelastic lithosphere, then the ratio $k_2^T(LT, s = 0)/k_2^T(LT = 0, s = 0)$ will approach 1.0, and the system (with $k_{nh} = 0$) will become unstable (as in Fig. 1A) for times longer than the decay time of the viscoelastic lithosphere. In contrast, for times less than this characteristic relaxation time, the system will behave according to Fig. 1(B). In other words, once the viscoelastic lithosphere relaxes, the bulge is free to adjust perfectly to the new position of the rotation vector, and the system loses memory of its original rotational state. This high-viscosity lithosphere case thus serves as a bridge between the stable state described in the theory of Willemann (1984) and Matsuyama *et al.* (2006), and the unstable state described by Gold (1955).

Finally, we note that any excess ellipticity will guarantee that the rotation remains stable, regardless of the relationship between $k_2^T(LT, \nu, s)$ and $k_2^T(LT = 0, s = 0)$ as $s \to 0$. Thus, an excess ellipticity will contribute a stabilization to the rotation. The Earth's current background form has an excess ellipticity equal to about 1 per cent of the hydrostatic value (Nakiboglu 1982), and this extra flattening is generally taken to be due to upwelling megaplumes below southern Africa and the Pacific (Lithgow-Bertelloni & Silver 1998). This raises a subtle point. If we were to use our theory to consider short timescale TPW (i.e. TPW of timescale 1 Myr or less) driven by mantle convection, then, since these megaplumes are unlikely to adjust non-negligibly over this time period, it would be appropriate to retain the term k_{nh} as it appears in the Liouville eq. (8). The convection induced changes in the inertia tensor over such timescales would thus be considered perturbations on the long-wavelength form associated with the more stable megaplumes. However, for long timescales, the excess ellipticity term should be interpreted as being part of the load-induced perturbation in the inertia tensor [i.e. part of $1 + k_2^L(LT, \nu, s)$], and it would not be appropriate to retain it in the Liouville eq. (8). In this case, we would set $k_{nh} = 0$ in this equation. The latter would also be the case for a realistic simulation of mantle convection that captured both the short- and long-term perturbations to the inertia tensor.

2.1 Establishing a range of validity for the Liouville equation

The question arises: how much TPW can occur before the linearization adopted to derive the Liouville eq. (8) breaks down? To quantify this issue, we will consider the final state of the scenario shown in Fig. 1(B5), where a surface mass load is applied and retained for all time on a rotating Earth model with a hydrostatic form and an initially unstressed elastic lithosphere. In particular, we will compare the $t = \infty$ response predicted using the Liouville eq. (8) (with k_{nh} set to 0) with the result based on the equilibrium, non-linear theory described by Matsuyama *et al.* (2006), following Willemann (1984). We begin with the latter.

Let us assume that an axisymmetric disk load is placed on the Greenwich meridian at some colatitude θ_L at time $t = 0$. Let us furthermore assume that the load can be represented in terms of a spherical harmonic decomposition,

$$L(\theta, \psi, t) = H(t) \sum_{\ell=0}^{\infty} \sum_{m=-\ell}^{\ell} L_{\ell m} Y_{\ell m}(\theta, \psi), \tag{10}$$

where $H(t)$ is the Heaviside function, θ is the colatitude, ψ is the east longitude and ℓ and m are the spherical harmonic degree and order, respectively. We assume that the spherical harmonic basis functions are normalized such that

$$\int_S Y^{\dagger}_{\ell' m'}(\theta, \psi) Y_{\ell m}(\theta, \psi) dS = 4\pi \delta_{\ell \ell'} \delta_{m m'}, \tag{11}$$

where † denotes a complex conjugation, and S represents an integration over the unit sphere.

If the same axisymmetric load was rotated to be centred on the north pole, then the spherical harmonic coefficients of this load (which we will denote by a superscript prime) would be related to the original harmonic components by

$$L_{2m} = L'_{20} \frac{Y^{\dagger}_{2m}(\theta_L, \psi_L = 0)}{\sqrt{5}}. \tag{12}$$

The spherical harmonic $\ell = 2, m = 0$ coefficient of the geopotential due to the direct gravitational effect of the surface mass (polar) load is given by (Matsuyama *et al.* 2006)

$$G^L_{20} = \frac{4\pi a^3 g}{5M} L'_{20}, \tag{13}$$

while the same harmonic coefficient of the geopotential associated with the background hydrostatic form of the model Earth is

$$G^H_{20} = -\frac{1}{3\sqrt{5}} a^2 \Omega^2 k_2^T(LT = 0, s = 0). \tag{14}$$

Following Willemann (1984) and Matsuyama *et al.* (2006), we thus define a normalized load size, Q', by the ratio

$$Q' = -\frac{G^L_{20}}{G^H_{20}} = \frac{\frac{4\pi a^3 g}{5M} L'_{20}}{\frac{1}{3\sqrt{5}} a^2 \Omega^2 k_2^T(LT = 0, s = 0)}. \tag{15}$$

With this definition in hand, the TPW angle δ for a load of normalized size Q' placed at a colatitude of θ_L is given by (Matsuyama *et al.* 2006)

$$\delta = \frac{1}{2} \arctan\left[\frac{Q' \alpha \sin(2\theta_L)}{1 - Q' \alpha \cos(2\theta_L)} \right], \tag{16}$$

where α is given by

$$\alpha = \frac{1 + k_2^L(LT, s = 0)}{1 - \frac{k_2^T(LT, s=0)}{k_2^T(LT=0, s=0)}}. \tag{17}$$

The parameter α is a function of the fluid ($s = 0$) state of both the Earth model and background hydrostatic form. For realistic Earth models, α is of order 1, and is only weakly sensitive to the choice of LT.

In Fig. 2 , we plot the TPW angle δ as a function of the initial load colatitude for five different values of $Q'\alpha$, ranging from 0.1 to ∞. The physics of this solution space is discussed in detail in Matsuyama *et al.* (2006). For loads of very large size, the TPW angle is $90^\circ - \theta_L$, and thus the final load position is always the equator. In this case, the load is so large that, despite the resistance of the remnant rotational bulge, the reorientation is governed by the stability theory described by Gold (1955) (Fig. 1A). However, for loads equal to 10 per cent of the size of the bulge, the TPW angle is less than a few degrees, no matter where the load is initially placed.

Next, we solve for the TPW using the Liouville eq. (8). In this case, the $I^L_{13}(t)$ inertia perturbation due to the load can be written as $I^L_{13} H(t)$. Moreover, with no loss of generality, we can express the time dependence in the m_1 component of the perturbation in the rotation vector as a series of N Heaviside load increments

$$m_1(t) = \sum_{n=0}^{N} \delta m_1^n H(t - t_n)\,. \tag{18}$$

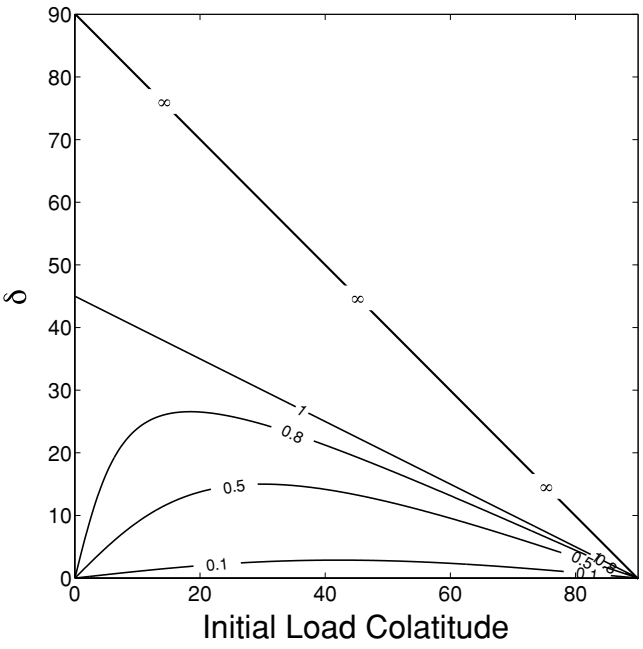

Figure 2. Predictions of TPW angle (δ) versus the initial colatitude of the loading for a suite of different $Q'\alpha$, as labelled on the contours. The calculations are based on eq. (16) derived using the equilibrium, non-linear theory of Matsuyama *et al.* (2006), after Willemann (1984).

Applying these expressions in (8) and performing the time convolution yields, using eq. (3),

$$\left(1-\frac{k_2^{T,E}}{k_2^T(LT=0,s=0)}\right)\sum_{n=0}^{N}\delta m_1^n H(t-t_n)$$
$$=\frac{{I_{13}}^L}{C-A}H(t)\left[1+k_2^{L,E}+\sum_{j=1}^{J}\frac{r_j'}{s_j}\left(1-e^{-s_j t}\right)\right]$$
$$+\frac{1}{k_2^T(LT=0,s=0)}\sum_{n=0}^{N}\delta m_1^n H(t-t_n)\sum_{j=1}^{J}\frac{r_j''}{s_j}\left(1-e^{-s_j(t-t_n)}\right)\ . \tag{19}$$

Setting $t=\infty$ in this equation, and using eq. (4), yields, after some simplification

$$m_1(t=\infty)=\frac{I_{13}^L}{C-A}\frac{1+k_2^L(LT,s=0)}{1-\frac{k_2^T(LT,s=0)}{k_2^T(LT=0,s=0)}}=\frac{I_{13}^L}{C-A}\alpha\ . \tag{20}$$

We could have arrived at the same result by using the $s\rightarrow 0$ limit in eq. (9).

One can show, using the definition in eq. (15) that

$$I_{13}=-\frac{1}{2}(C-A)Q'\sin(2\theta_L). \tag{21}$$

Using this expression in eq. (20) yields

$$m_1(t=\infty)=-\frac{1}{2}Q'\alpha\ \sin(2\theta_L), \tag{22}$$

and therefore, the predicted amplitude of TPW based on the linearized theory is

$$\delta=\tan^{-1}\left(\frac{1}{2}Q'\alpha\ \sin(2\theta_L)\right). \tag{23}$$

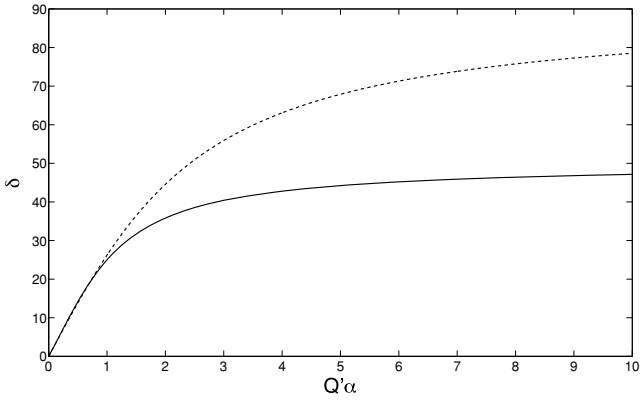

Figure 3. Predictions of the TPW angle (δ) versus $Q'\alpha$ generated using the (solid line) equilibrium, non-linear theory of Matsuyama *et al.* (2006), following Willemann (1984) (eq. 16) and the (dashed line) linearized theory (eq. 23).

We now have two expressions for the TPW associated with the scenario in Fig. 1(B): eq. (23), based on the asymptotic value of our linearized rotation theory in response to a Heaviside loading; and a value computed using an equilibrium (i.e. no time-dependence) non-linear stability theory, eq. (16). In both cases, the required Earth model structure in the fluid limit is embedded in the parameter α (eq. 17). A comparison of the results generated using the linearized and non-linear theories will provide a quantitative measure of the accuracy of the former in predictions of TPW.

As an illustration of this accuracy, Fig. 3 shows predictions of TPW versus $Q'\alpha$ predicted using the non-linear (solid line) and the linearized (dashed line) stability theories for a load placed on the Earth at an initial colatitude of 40°. At $\delta=20^\circ$ ($Q'\alpha\sim 1$), the prediction based on the linearized theory has an error of less than 5 per cent. This error increases to about 10 per cent for a TPW of 30° ($Q'\alpha\sim 1.5$). The accuracy of the linearized theory degrades monotonically for higher $Q'\alpha$ values.

We next generalize this analysis to consider a range of θ_L values in Fig. 4. Fig. 4(A) shows contours of TPW (δ) for $0^\circ<\theta_L<90^\circ$ and $Q'\alpha<1$, predicted using the linearized theory. Fig. 4(B) plots the associated error in these predictions. It is clear from the figure that the accuracy of the linearized theory is greatest when the load is placed at mid-latitudes. For $40^\circ<\theta_L<50^\circ$, predictions of $\delta\sim 20^\circ$ that are obtained for $Q'\alpha\sim 1$ have an error less than 30 per cent. In reference to Fig. 2, we note that this preferred range of θ_L samples the region where $\partial(\delta)/\partial\theta_L$ is smallest, at least for $Q'\alpha<0.1$.

We conclude from this section that by applying a load to the Earth model at mid-latitudes, the linearized stability theory will be accurate to order 10 per cent for TPW predictions up to 20°. This will serve as a guideline for the numerical tests described in the next section.

3 RESULTS AND DISCUSSION

In this section, we turn to an examination of the rotational stability of the Earth in response to a time-varying perturbation in its inertia tensor. The term $\mathbf{I}^L(t)+k_2^L(LT,\nu,t)*\mathbf{I}^L(t)$ in the governing eq. (8) incorporates both the load and its isostatic compensation. In considering loads associated with mantle convection, we will impose

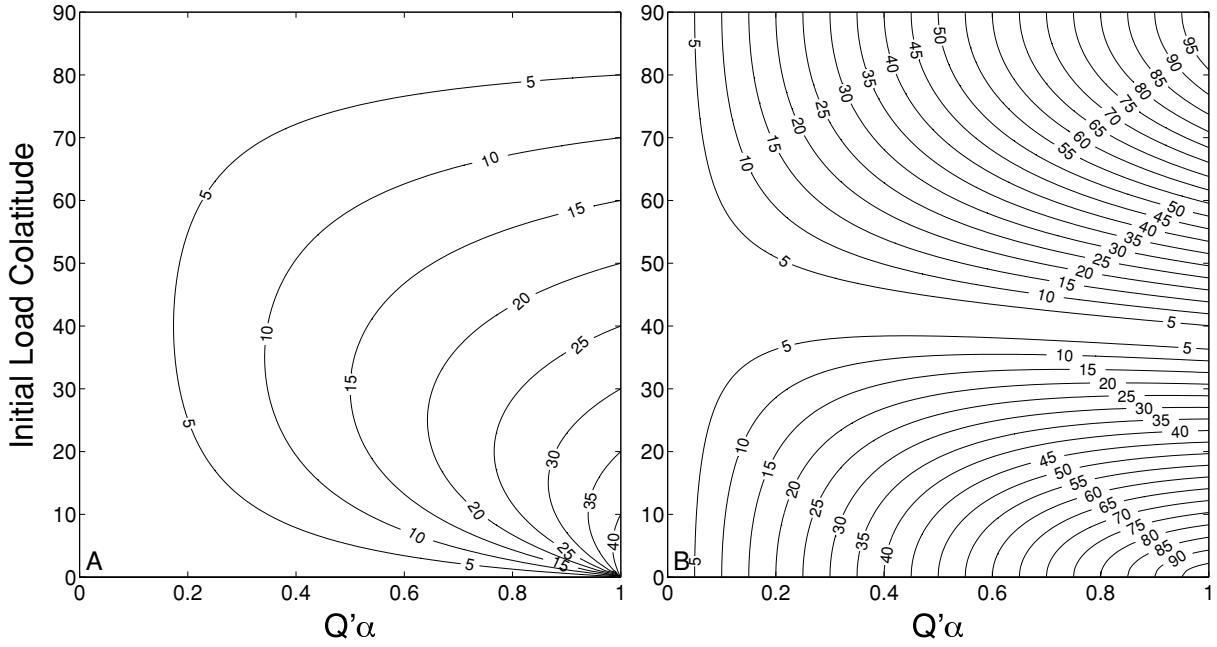

Figure 4. (A) Predictions of the TPW angle (δ), as labelled on the contours, in a solution space that varies the initial colatitude of the load, θ_L, and $Q'\alpha$. Calculations are based on eq. (23). (B) Percent error in the predictions generated using the linearized rotational stability theory (frame A) computed via a comparison with the expression (16).

this total 'effective' load, and we can thus rewrite this equation as

$$\mathbf{m}(t) = \frac{\mathbf{I}_{\rm eff}(t)}{(C-A)} + \frac{k_2^T(LT, \nu, t)}{k_2^T(LT=0, s=0) + k_{nh}} * \mathbf{m}(t). \tag{24}$$

As discussed above, this form incorporates the stabilizing influence of the remnant rotational bulge and, for $k_{nh} \neq 0$, any excess ellipticity in the Earth's form. As discussed below eq. (9), the special case of time-domain eq. (8) consistent with the physics first described by Gold (1955) is obtained by setting k_{nh} to 0, and using an Earth model with no purely elastic component of the lithosphere

$$\mathbf{m}(t) = \frac{\mathbf{I}_{\rm eff}(t)}{(C-A)} + \frac{k_2^T(LT=0, \nu, t)}{k_2^T(LT=0, s=0)} * \mathbf{m}(t). \tag{25}$$

In this case, an uncompensated load will ultimately reach the equator, as in the scenario in Fig. 1(A), although in our linearized theory this instability will be manifest in an unbounded TPW. In the following discussion we will use the terms 'new theory' and 'traditional theory' when referring to solutions based on eqs (24) and (25), respectively. We emphasize, however, that our eq. (25) provides the time-dependence of the system in Fig. 1(A), in contrast to the usual equilibrium form of the traditional theory (Gold 1955) adopted in most previous mantle convection studies, which specifies only the final state of the pole.

The Maxwell viscoelastic Earth we adopt is spherically symmetric and self-gravitating. The elastic and density structure of the model is given by the seismically inferred model PREM (Dziewonski & Anderson 1981). The viscosity structure is discretized into three layers: an elastic (i.e. infinite viscosity) lithosphere of thickness LT, an upper mantle viscosity set to 10^{21} Pa s, and a lower mantle viscosity that will vary in the simulations.

Finally, we need to prescribe the effective inertia tensor perturbation or, using eq. (21), the normalized load size Q' and load colatitude θ_L. Following the arguments of the last section, we will adopt $\theta_L = 40^\circ$ to optimize the accuracy of the linearized theory, and this yields

$$Q' = \frac{2\bar{\mathbf{I}}_{\rm eff}}{(C-A)\sin 80^\circ}, \tag{26}$$

where $\bar{\mathbf{I}}_{\rm eff}$ is the maximum value in the time variation of $\mathbf{I}_{\rm eff}(t)$.

What is an appropriate value of Q'? That is, what is the expected normalized load associated with mantle convection over the timescales of interest to our study ($\sim$1 Myr)? To estimate this load, we begin by considering the total perturbation in the Earth's present-day figure due to mantle flow, which we can approximate using two lines of reasoning. First, the excess ellipticity of the Earth is recognized as being the consequence of two large scale megaplumes within the mantle (Lithgow-Bertelloni & Silver 1998). Hence, $k_{nh}/k_2^T(LT=0, s=0)$ (see eq. 7)—that is, the ratio of the excess and hydrostatic ellipticity—thus provides one measure of the net normalized load due to mantle flow. For the Earth models described above, $k_2^T(LT=0, s=0) = 0.9342$, and $k_{nh} = 0.008$ from Nakiboglu (1982), and hence this ratio is $\sim$0.0086 (or 0.86 per cent). Alternatively, the difference in the Earth's two principal equatorial moments of inertia, $(B-A)$, is also presumably due to mantle convection, and the observed ratio $(B-A)/(C-A) \sim 0.007$ (Gross 2007). It is reasonable to assume that this ratio would also be approximately equal to the fractional contribution of convection to the observed $C-A$, and thus it provides a second, consistent estimate of the total normalized load due to convection.

Now, the timescale for density heterogeneities to complete a circuit through a whole mantle convection cell is, using surface plate speeds as an estimate for the characteristic flow velocity, approximately 100 Myr. This suggests that, over a timescale of 1 Myr, the variation in the normalized load due to mantle flow will be of order 1 per cent of the total, or $\sim 8 \times 10^{-5}$. To be conservative, our 'standard test case' will be 10 times this value, $Q' = 0.0008$. While we will consider the sensitivity of the TPW predictions to a variation in the load size, it is important to emphasize that the

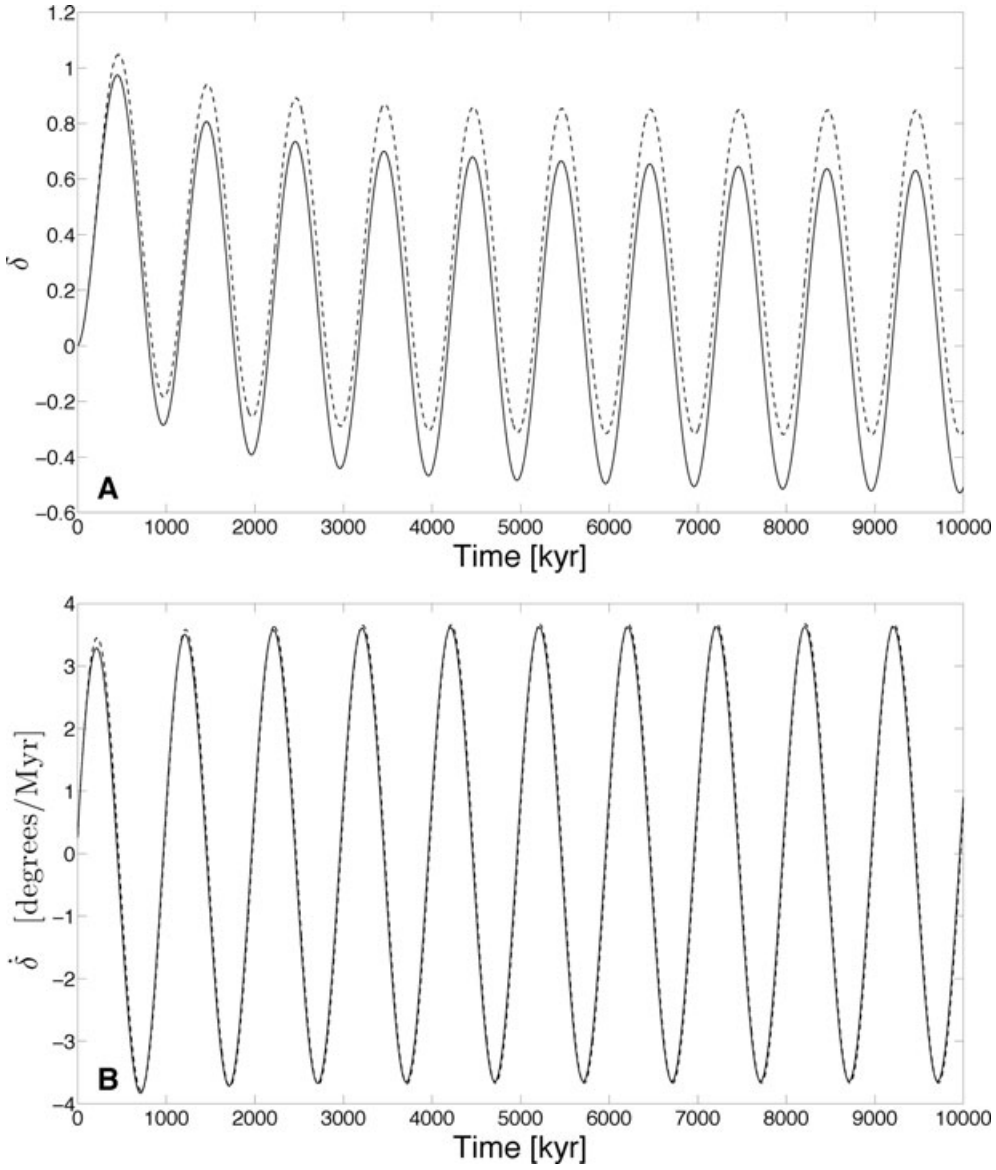

Figure 5. Predicted (A) TPW and (B) TPW rate versus time computed using (dotted line) our time dependent treatment of the traditional rotation physics (eq. 25), and the (solid line) new rotation theory which includes stabilization associated with the remnant rotational bulge (eq. 25) with k_{nh} set to zero. All other aspects of the solution are based on the standard test case: $LT = 25$ km, $\nu_{\rm LM} = 10^{22}$ Pa s, $Q' = 0.0008$ and $\tau_c = 1$ Myr. The time dependence of the inertia tensor perturbation is given by eq. (27).

standard test case represents a ∼10 per cent variation in the excess ellipticity over timescales of just ∼1 Myr.

The standard test case will also be defined by an Earth model with LT =25 km, a lower mantle viscosity (henceforth $\nu_{\rm LM}$) of 10^{22} Pa s, and $k_{nh} = 0$. In regard to the convection signal, we will assume two forms of time dependence. The first is a sinusoidal forcing,

$$\frac{\mathbf{I}_{\rm eff}(t)}{\bar{\mathbf{I}}_{\rm eff}} = \sin(2\pi t/\tau), \tag{27}$$

where $\tau = 1$ Myr in the standard case. The second has the form

$$\frac{\mathbf{I}_{\rm eff}(t)}{\bar{\mathbf{I}}_{\rm eff}} = \big\{\tanh[A(t-B)] + 1\big\}/2, \tag{28}$$

where $A = 6$ Myr^{-1} and $B = 0.5$ Myr in the standard run. In this case, the right hand side of eq. (28) increases from a value of 0 to 1 in 1 Myr. We will perform a sequence of sensitivity analyses in which $\nu_{\rm LM}$, LT, τ and k_{nh} are varied.

3.1 Periodic forcing

To begin, Fig. 5 shows a prediction of TPW and TPW rate as a function of time for the standard test case. The results are generated using (solid line) the new rotation theory that accounts for the stabilization due to the remnant bulge (eq. 24 with $k_{nh} = 0$) and (dashed line) the theory in which this stabilization is absent (eq. 25). It is clear from the figure that the remnant bulge stabilization does not contribute significantly to either the TPW or its rate of change for a sinusoidal loading with period of $\tau = 1$ Myr.

In Fig. 6, we explore the sensitivity of the TPW prediction in the standard test case solution to variations in the normalized load size Q', the excess ellipticity k_{nh}, the period τ of the forcing, and the adopted lower mantle viscosity $\nu_{\rm LM}$. We also performed an analysis (not shown) in which the elastic lithospheric thickness, LT, was varied from the standard value (25 km). This latter analysis,

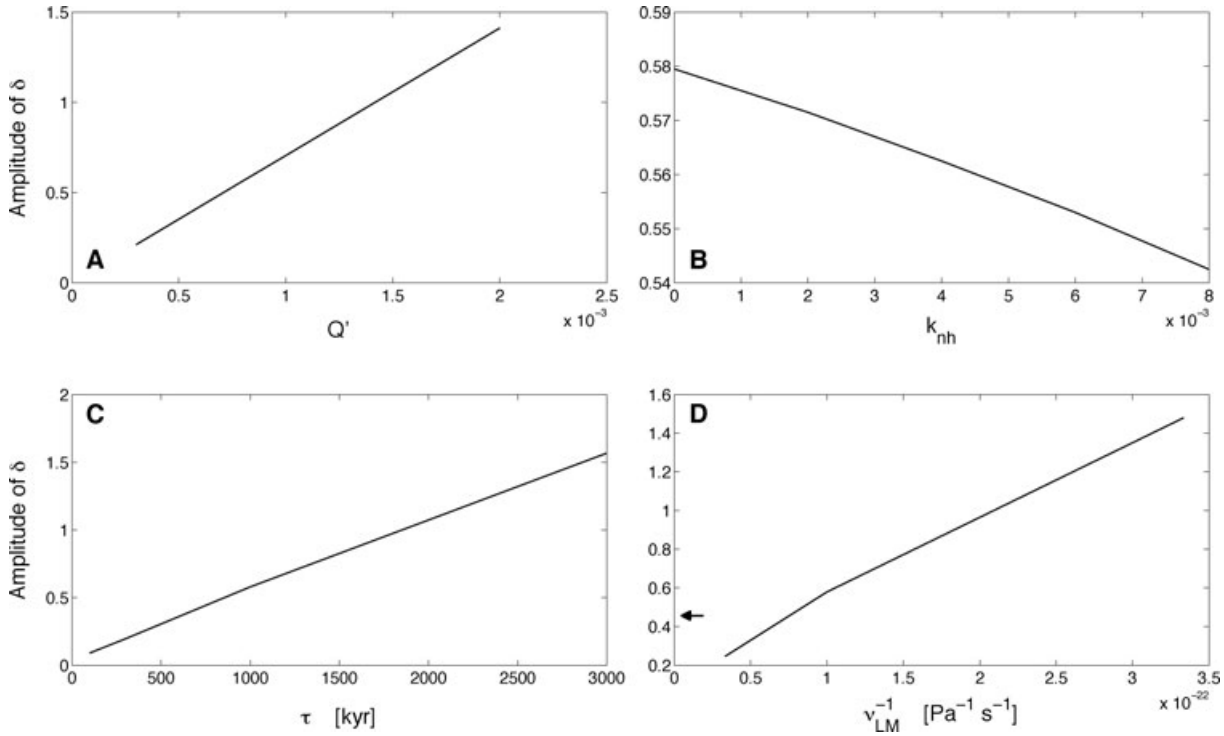

Figure 6. Predicted TPW amplitude (half the peak-to-peak variation) as a function of the (A) normalized load size Q', (B) the adopted background excess ellipticity k_{nh}, (C) the period τ_c of the sinusoidal perturbation to the inertia tensor ($I_{\rm eff}$) and (D) the adopted lower mantle viscosity, $\nu_{\rm LM}$. Calculations adopt the new rotation theory (eq. 25) and, with the exception of the parameter being varied, the solutions are based on the standard test case values: $LT = 25$ km, $\nu_{\rm LM} = 10^{22}$ Pa s, $Q' = 0.0008$ and $\tau_c = 1$ Myr. The arrow in frame D indicates the amplitude predicted in a calculation in which we adopt the viscosity profile inferred from a joint inversion of ice age and convection data sets (see text).

as well as the results associated with varying k_{nh} (Fig. 6B), show relatively little sensitivity to a variation in the associated parameter, and this generalizes the conclusion we reached on the basis of Fig. 5; namely, the amplitude and TPW rate for a forcing of period ∼1 Myr are insensitive to the stabilization associated with either a remnant rotational bulge or a stable (on the timescale of the forcing) excess ellipticity.

The remaining results in Fig. 6 confirm the general sensitivities identified by Tsai & Stevenson (2007). In particular, the amplitude of the TPW, and the peak rate of change (which can be inferred, in units of deg Myr^{-1}, from Fig. 6 by multiplying the y-axis values by a factor of ∼4.5), are linearly sensitive to the loading amplitude and the period of the sinusoidal forcing, and they are inversely proportional to the lower mantle viscosity. The linear relationship between the predictions and Q' is, in fact, explicit in our governing eq. (24).

So, what is the amplitude and speed limit of TPW in response to a rapid, periodic forcing? Let us consider a loading timescale of $\tau \sim 1$ Myr. In this case, the standard run yields a maximum peak-to-peak amplitude of ∼1°, and a maximum speed (which is only attained for a short period of time) of 3.5 deg Myr^{-1}. As we have discussed, the standard Q' value we have adopted represents a variation in the mantle convective loading of 10 per cent of the total convective load over a specified timescale τ. Simulations of mantle convection extending over the past 20 Myr indicate that over a 1 Myr timescale the peak variation in the convection-induced load is a fraction of 1 per cent of the total signal (see Forte & Mitrovica 1997, Fig. 3a), suggesting that our standard value for Q' is a very conservative upper bound. The standard run also adopted a lower mantle viscosity $\nu_{\rm LM} = 10^{22}$ Pa s. Recent, joint inversions of data related to ice age sea level adjustments and mantle convection (Mitrovica & Forte 2004) infer a mean deep mantle viscosity in excess of this value. On Fig. 6(D), we superimpose the predicted amplitude of TPW generated using this specific inference of viscosity—this calculation yields an amplitude about 15 per cent lower than the standard case. We note that some ice age studies have suggested a lower mantle weaker than 10^{22} Pa s (Peltier 2004). However, the data sets used in such analyses (e.g. relative sea level histories) are primarily sensitive to shallow lower mantle structure. Spherical harmonic degree 2 anomalies (e.g. TPW) will be sensitive to viscosity variations in the deep mantle, a region where ice age data sets provide limited radial resolution (Mitrovica 1996). Therefore, the lower mantle viscosity adopted in the standard run is also a conservative choice.

3.2 A gradual step change in the convective loading

Next, we consider TPW driven by a net change in the convective forcing defined by the time history in eq. (28). For the standard run ($A = 6.0$ Myr^{-1} and $B = 0.5$ Myr), this time history involves a ramp-up in the load from a value of 0 to Q' in 1 Myr, with the most rapid change in the middle 0.5 Myr of the loading phase. Beyond this phase, the load stays in place. The solid lines in Figs 7(A) and (B) are the predicted TPW and TPW rate computed using our (linearized) time-dependent form of the traditional rotational stability theory (eq. 25) with all parameters set to the standard test run case. As discussed above, the equilibrium theory of Gold (1955) (i.e. the final frame of Fig. 1A) will ultimately place the load on the equator, and since the load is positioned at a colatitude of 40°, this means a final TPW of 50°. In our linearized theory, the instability described

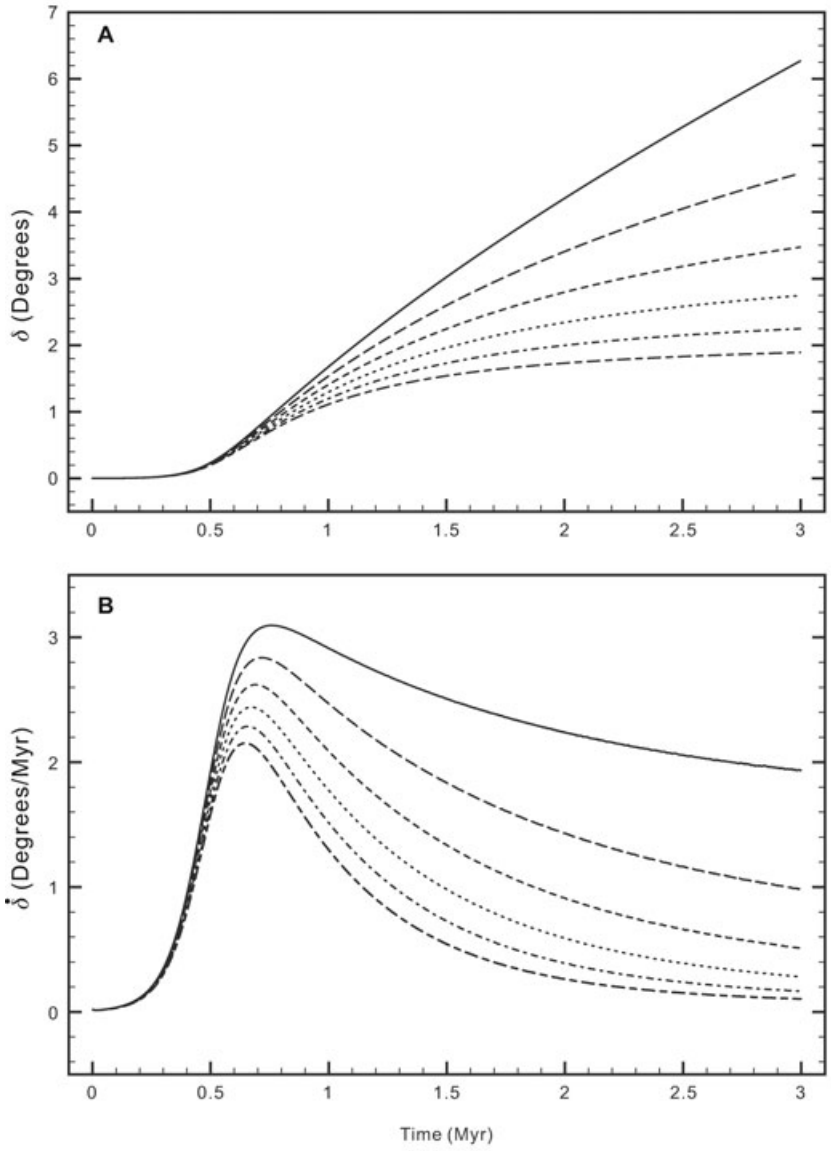

Figure 7. (A) TPW and (B) TPW rate versus time computed using the (solid line) time domain treatment of the traditional rotation theory (eq. 25), and the new rotation theory (eq. 24) with k_{nh} set to either (long-dashed line) 0.0 (the standard test case), (short-dashed line) 0.002, (dotted line) 0.004, (dashed-dotted line) 0.006 or (long-dashed-short-dashed line) 0.008. All other aspects of the solution are based on the standard test case: $LT = 25$ km, $\nu_{\rm LM} = 10^{22}$ Pa s, $Q' = 0.0008$, and time dependence of the inertia tensor perturbation is given by eq. (28) with $A = 6$ and $B = 0.5$.

in the context of Fig. 1(A) leads to an unbounded TPW, although we will focus our attention on the time history well within the linear regime mapped out by Figs 2–4.

Two million years after the load is fully emplaced, the net TPW has reached 6° and the TPW rate is 2 deg Myr^{-1}. At 10 Myr from the onset of loading (not shown), these values are 18.2° and $\sim$ 1.65 deg Myr^{-1}, respectively. This suggests that the time required for the load to reach close to the equator, for the suite of parameters that define the standard test case, is at least 50 Myr.

The long-dashed line in each frame of Fig. 7 represents a prediction based on the new rotation theory that incorporates the stabilization of the rotation pole associated with the remnant bulge (eq. 24 with $k_{nh} = 0.0$). In contrast to the case of sinusoidal loading, this stabilization has a pronounced impact on the reorientation of the rotation pole. Two million years after the full load is established, the pole has reached $\sim$4.5°, and the TPW rate has dropped to 1 deg Myr^{-1}, or half the rate predicted in the absence of the stabilization due to the remnant bulge. At 10 Myr after the onset of loading (not shown), the TPW rate has fallen to 0.3 deg Myr^{-1}, and the net TPW has reached 8.4°.

The remaining predictions in Fig. 7 illustrate the progressively stronger stabilization of the rotation pole as the remnant bulge physics is augmented by successively higher amplitudes of stable (over the 3 Myr timescale covered by the plot) excess ellipticity. Indeed, in the 3 Myr since the onset of the loading, the predicted TPW for the most stable case, with an adopted excess ellipticity equal to the present-day value ($k_{nh} = 0.008$, as discussed above), has essentially ceased and the final reorientation is $\sim$2°. We note that the present-day, non-hydrostatic figure of the Earth is triaxial, and the excess ellipticity values in the direction of the two principal equatorial axes are actually 0.0115 and 0.0052 (Matsuyama *et al.* 2010) (the average of these to numbers gives the 0.008 value quoted above); thus the precise level of stabilization would, in the case of a triaxial figure, be a function of the direction of the TPW.

We conclude from Fig. 7 that during periods of relative hiatus in the variability of the convective loading, ongoing TPW predicted on the basis of the traditional rotational stability theory (eq. 25) may be a significant overestimate. Stabilization associated with both a remnant rotational bulge and an excess ellipticity which remains stable over the period of the hiatus will both strongly inhibit TPW. It is important to note that the stabilization associated with the excess ellipticity is independent of the remnant bulge stabilization. That is, although the four lower lines in each frame of Fig. 7 consider the two effects in tandem, we could have alternatively considered the excess ellipticity stabilization in the absence of the remnant bulge stabilization associated with the elastic lithosphere.

In Fig. 8, we return to the standard test case (long dashed lines in the frames of Fig. 7) and consider the sensitivity of the predictions to (from first to last row) the normalized size of the load (Q'), the timescale of loading, the lower mantle viscosity and the thickness

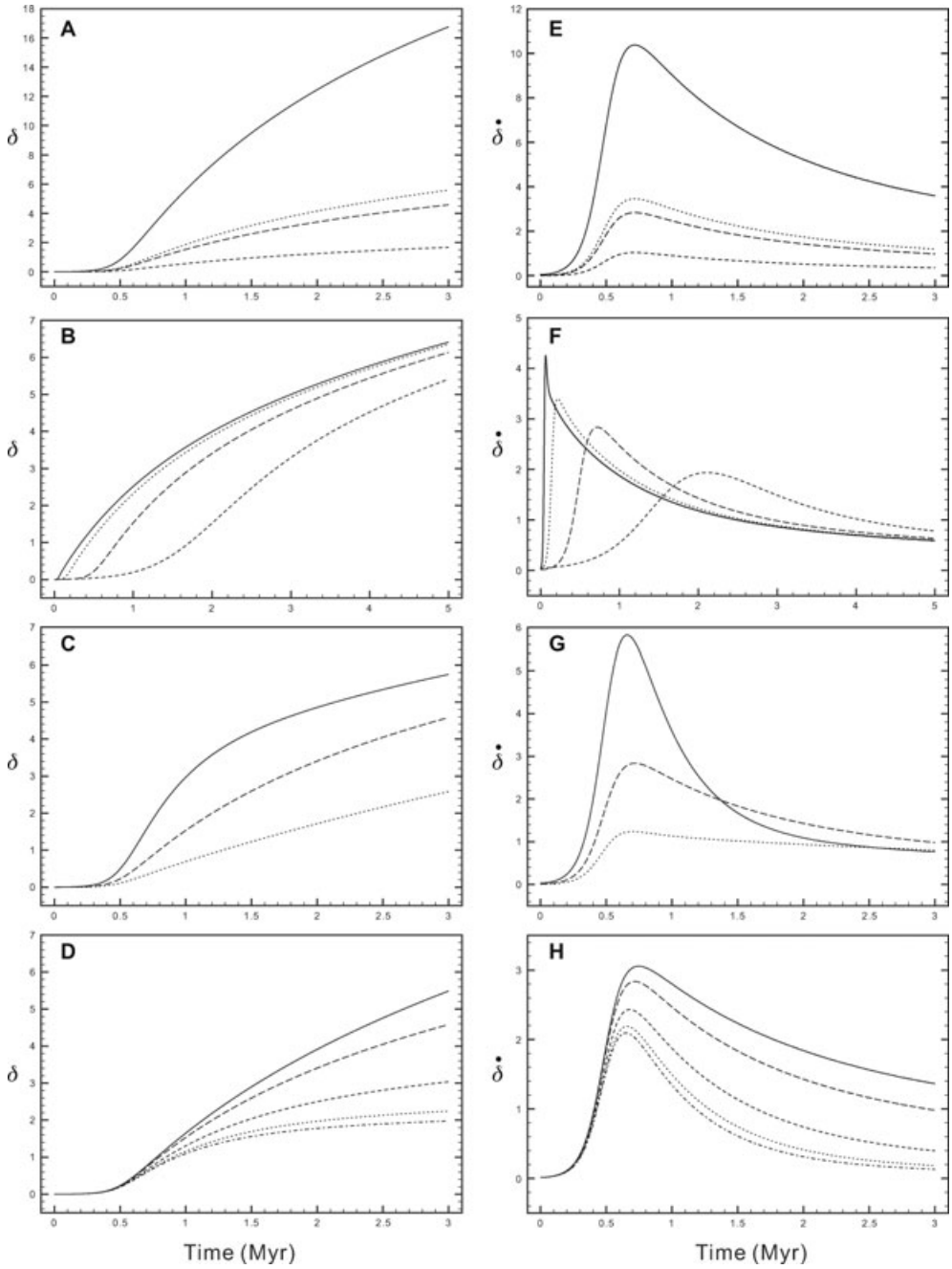

Figure 8. Predicted (left column) TPW and (right column) TPW rate versus time for a suite of predictions in which individual parameters are varied from the value which defines the standard test case. All calculations are based on the time-domain eq. (24), with k_{nh} set to zero, and the time-history of loading given by eq. (28). (A,E) Q' varied from (solid line) 0.003, (dotted line) 0.001, (long-dashed line) 0.0008 and (short-dashed line) 0.0003. (B,F) Ramp-up timescales of (solid line) 100 kyr, (dotted line) 300 kyr, (long-dashed line) 1 Myr and (short-dashed line) 3 Myr. (C,G) $\nu_{\rm LM}$ varied from (solid line) 3×10^{21} Pa s, (long-dashed line) 10^{22} Pa s, and (dotted line) 3×10^{22} Pa s. (D,H) LT varied from (solid line) 10 km, (long-dashed line) 25 km, (short-dashed line) 46 km, (dotted line) 67 km and (dashed-dotted line) 88 km. With the exception of the parameter being varied, the solutions are based on standard test case values: $LT = 25$ km, $\nu_{\rm LM} = 10^{22}$ Pa s, $Q' = 0.0008$ and $\tau_c = 1$ Myr.

of the elastic lithosphere. In all cases, we use the time-domain eq. (24) with $k_{nh} = 0$.

In the top row we explore the impact of varying Q' from 0.0003 to 0.003. As discussed above in the context of the periodic forcing, the predictions of TPW and TPW rate for the ramp-up forcing should be linearly related to Q' (eq. 24), and this is clearly evident in Fig. 8. As an example, at 700 kyr, the net TPW rate predictions for $Q' = 0.0003$ and 0.003 are 1 deg Myr^{-1} and $\sim$ 10 deg Myr^{-1}, respectively.

The sensitivity of TPW and TPW rate predictions to variations in the timescale over which the load is applied (second row, Fig. 8) is relatively small once $\sim$3 Myr have elapsed. Peak TPW speeds are obtained in the latter part of the loading ramp-up, and the amplitude of this peak decreases as the ramp-up period increases, from 4.2 deg Myr^{-1} for the 0.1 Myr ramp-up case to 2 deg Myr^{-1} for the case of a 3 Myr ramp up. Significantly, 5 Myr after the onset of loading, the TPW rate for all four cases treated in Fig. 8(F) have converged to just under 1 deg Myr^{-1}.

The third row of Fig. 8 considers the impact on the TPW predictions of increasing the lower mantle viscosity by an order of magnitude. During the loading ramp up, both the TPW and TPW speed decrease monotonically with increasing $\nu_{\rm LM}$. However, as the ramp-up slows, and in the period after the ramp up, the predicted TPW speeds decay at different rates and by 3 Myr they have converged to nearly the same value as in Fig. 8(F): 1 deg Myr^{-1}. What is causing this transition from the early sensitivity to viscosity to the latter insensitivity? During the initial onset of the load, TPW is limited by the ability of the bulge to readjust and this, in turn, is governed by the lower mantle viscosity—the higher the viscosity, the more sluggish the adjustment. However, after a relatively modest level of TPW has occurred, the stabilizing impact of the remnant bulge associated with the elastic lithosphere, which will increase with increasing TPW, becomes dominant, and this stabilization is insensitive to lower mantle rheology. Hence, the predicted TPW rates will converge in this interval.

This transition from a TPW response dominated by viscous bulge adjustment to remnant bulge stabilization is evident schematically in Fig. 1, where in the first few columns of the figure the TPW path is similar for both scenarios. As time progresses and the remnant bulge stabilization takes over, the TPW in the second scenario is significantly more muted than in the first case. The transition also explains why, after the ramp-up in loading, TPW rates converge to a roughly similar value (1 deg Myr^{-1}); the stabilizing impact of the remnant bulge is not only insensitive to the lower mantle viscosity, it is also insensitive to the period over which a load of normalized size Q' is built up. Of course, since the ultimate location of the pole is governed by a balance between the load size and the remnant bulge stabilization, the curves in Fig. 8(E) will exhibit more sensitivity than those in Figs 8(F) and (G) in the period after the load is fully in place; however, each of these curves will eventually converge to zero as the polar motion ceases (i.e. at the point where the strength of the load and the stabilization strength become equal).

In the final row of Fig. 8, we consider the sensitivity of the predictions to changes in the thickness of the elastic lithosphere. As one increases the lithospheric thickness, one increases the strength of the remnant bulge, and hence the predicted TPW remains a strong function of the adopted value of LT well after the load ramp-up; this is also reflected in the predicted TPW rates, which show significant differences 3 Myr after the onset of loading. Once again, this sensitivity contrasts with results based on the sinusoidal forcing.

The predictions in Fig. 8 adopt $k_{nh} = 0$, and thus they do not include any stabilization associated with a background excess ellipticity. As discussed above, the present-day excess ellipticity of the Earth along the intermediate and minimum axes of inertia are 0.0052 and 0.0115, respectively. We do not know how this convection signal has varied in the past; however, it will always be true, as discussed in the context of Fig. 1, that the rotation vector will tend to reorient such that any excess ellipticity moves toward the equator. In any event, for the sake of illustration, and to be conservative, in Fig. 9 we repeat the simulations in Fig. 8 with k_{nh} set to 0.004. To facilitate comparison, Fig. 9 is drawn using the same scales as Fig. 8.

Introducing this relatively modest level of excess ellipticity yields a net TPW at 5 Myr that is only about half the total TPW predicted in the absence of this stabilization. During the ramp up in the loading, the TPW and TPW rate are less sensitive to the choice of k_{nh}; however, the discrepancies grow during the period in which the loading is complete. This is yet another manifestation of the transition from a load-dominated TPW phase to a phase in which the stabilizing effects of the remnant bulge and the excess ellipticity begin to dominate.

Using the results in this section, we can reassess the inference by Sager & Koppers (2000) of 16°–21° of TPW in 2–5 Myr during the Late Cretaceous. Let us assume that this reorientation was due to a net shift in the convective loading. The results in Figs 8(B) and 9(B) demonstrate that TPW over this time period would be relatively insensitive to the timescale of the ramp-up in the convective load. In the absence of any stabilization due to excess ellipticity, the predictions in Fig. 8(A) indicate that TPW of this amplitude would require a convective load of $Q' \sim 0.003$. Adopting an excess ellipticity of $k_{nh} = 0.004$ (Fig. 9A) increases the size of the required load by about 60 per cent, that is, $Q' = 0.005$. (The Earth's excess ellipticity 85 Ma is unknown; however, the size of the megaplume structures below Africa and the Pacific suggest that this convectively supported contribution to the oblateness of the Earth may not have been significantly different from today's value. Therefore, in this case, adopting $k_{nh} = 0.004$ is likely an underestimate.) The required load size would be only marginally smaller if we adopted a lower mantle viscosity as low as 3×10^{21} Pa s (Figs 8C and 9C) or an elastic lithospheric thickness as thin as 10 km (Figs 8D and 9D). The palaeomagnetic inference of Sager & Koppers (2000) thus requires that a convective forcing on the order of the size of the current excess ellipticity of the Earth must have been applied in a timescale of a few million years. We conclude, on this basis, that the palaeomagnetic inference is physically implausible.

4 FINAL REMARKS

Using recent results in ice age theory (Mitrovica *et al.* 2005), we have derived a linearized rotational stability theory that permits predictions of time-dependent TPW on a convectively loaded Maxwell Earth. A special case of the theory allows one to assess the time dependence of the rotation vector under assumptions consistent with the canonical equilibrium stability theory first described by Gold (1955) (Fig. 1A) and adopted in most previous analyses of convection-induced TPW. However, in its most general form, our theory augments this canonical treatment to include the possible stabilization of the Earth's rotation vector due to the remnant bulge associated with an elastic lithosphere and any excess ellipticity in the Earth's shape that is stable over the timescale of interest. The linearization is valid for small angles of TPW; however, we have demonstrated the conditions under which the error in the treatment is less than 5 per cent for TPW reaching 20°.

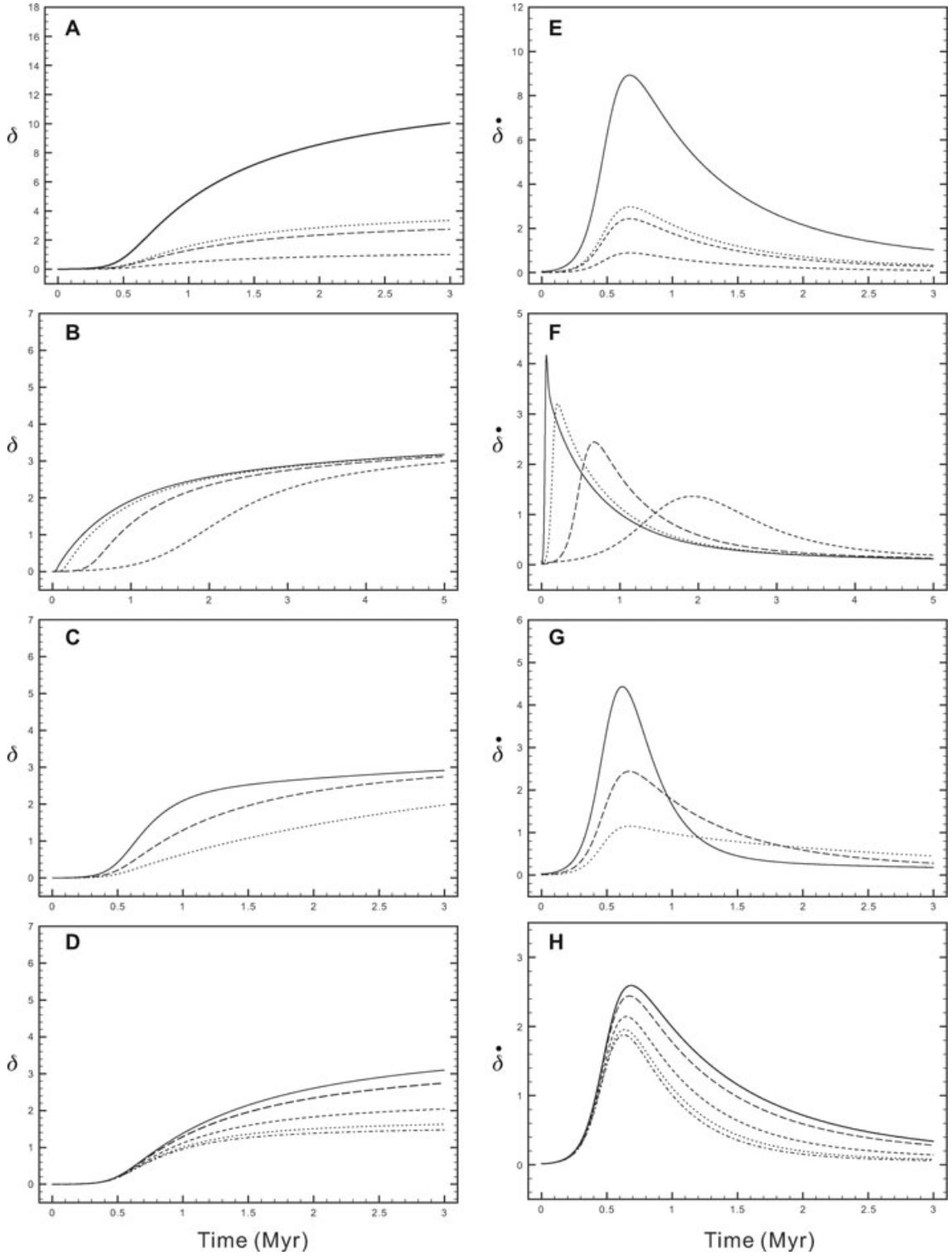

Figure 9. As in Fig. 8, except all calculations adopt $k_{nh} = 0.004$, and thus incorporate stabilization due to excess ellipticity.

As a first application of the theory, we have considered TPW in response to relatively rapid, ∼1 Myr, perturbations in the inertia tensor. In this regard, we have adopted two specific time histories: a periodic (sinusoidal) forcing, and a gradual ramp-up (hyperbolic tangent) forcing. The calculations using the periodic forcing have largely confirmed results by Tsai & Stevenson (2007), who concluded that the TPW angle and rate would be linearly proportional to the magnitude and period of the loading and inversely proportional to the adopted lower mantle viscosity. We have also demonstrated that these predictions are, within the parameter regime we have considered, insensitive to the stabilization associated with the remnant bulge or excess ellipticity. Using our predictions, we conclude that

TPW of amplitude $\sim 10^\circ$ with $\sim$1 Myr periodicity would require large—and in our view unrealistic—perturbations in the inertia tensor over this timescale. Indeed, these inferences suggest changes in the inertia tensor over timescales of 1 Myr that are much larger than 10 per cent of the perturbation implied by the Earth's present-day excess ellipticity.

Our predictions based on a step ramp up in the convection load show far greater sensitivity to the stabilization associated with the remnant bulge and excess ellipticity. More specifically, in the case of the load ramp-up, we note a transition from load-dominated TPW during the period of active loading to a phase, after loading is complete, in which the remnant bulge and excess ellipticity significantly limit polar motion. Indeed, these stabilizing factors are sufficient to stop the rotation pole far from the equatorial position expected on the basis of the canonical stability theory of Gold (1955). We should emphasize that this limit on TPW has been understood and applied within the literature of planetary rotation (e.g. Willemann 1984; Matsuyama *et al.* 2006; Daradich *et al.* 2008)—in this regard, the theory described herein extends these efforts to consider the time history of the evolution of pole position in the presence of these stabilization mechanisms. On the basis of these predictions, we have concluded that the inference of a 16°–21° reorientation of the rotation pole over 2–5 Myr during the Late Cretaceous is also implausible.

The predictions described here assume that the elastic lithosphere of the Earth is unbroken. As we discussed in Section 1, an important question that needs to be addressed is to what extent the 'effective elastic thickness' of the real Earth in response to a perturbed centrifugal potential differs from response of a model Earth with an unbroken elastic lithosphere of some thickness LT. As a preliminary assessment of this issue, we used a finite-element numerical procedure developed for ice age geodynamic problems (Latychev *et al.* 2005) to compare the 1 Myr response of: (1) an Earth model with an elastic lithosphere of thickness 100 km at all locations except at plate boundaries where (by virtue of a finite viscosity) the elastic thickness is zero, and (2) a sequence of Earth models with a uniform elastic thickness that is varied from 10 to 100 km. We found that the (spherical harmonic degree two, order one) response of the broken lithosphere model to a perturbation in the centrifugal potential arising from a 5° shift in the pole along the Greenwich meridian was the same as the response at the same degree and order of a uniform elastic lithosphere of thickness $LT \sim 60$ km. This suggests that the effective elastic thickness LT of the Earth in response to forcings on timescales of $\sim$1 Myr is a sizeable fraction of the mean lithospheric thickness, and that the standard value of $LT =$ 25 km we adopted in this study is a reasonable and conservative choice. Nevertheless, it is important to recall that the effective elastic thickness of the broken lithosphere, and hence the importance of the remnant bulge stabilization, will be a function of the timescale of the forcing. For example, analyses of TPW over timescales of 10s–100s of Myr would have to account for the fact that the creation of oceanic lithosphere near mid-ocean ridges sets the local form of the plate to the contemporaneous hydrostatic figure. A conservative test of the effective elastic thickness of the lithosphere in this case might set the elastic strength of the oceanic component of the lithosphere to zero. Plate motions during TPW events may also play a role in establishing the strength of the remnant bulge stabilization over such timescales.

The normal mode treatment we have described provides a flexible methodology for investigating the impact on convection-induced TPW of a suite of other factors related to Earth structure. For example, our results have assumed that the lithosphere is characterized by infinite viscosity (i.e. that it is purely elastic). Adopting a finite viscosity lithosphere would introduce a normal mode with a relaxation time given by the Maxwell time of the lithosphere, and as we have noted this would lead to a transient remnant bulge stabilization. In addition, alternate linear rheologies can be treated without any additional complexity in the modelling. Finally, within the range of linearization, our theoretical methodology can be used to assess other aspects of the Earth's rotational stability in response to convective forcing. These include, for example, the relatively muted TPW inferred for the past few 100 Myr from palaeomagnetic data (Besse & Courtillot 2002; Steinberger & Torsvik 2008).

REFERENCES

Besse, J. & Courtillot, V., 2002. Apparent and true polar wander and the geometry of the geomagnetic field over the last 200 myr, *J. geophys. Res.,* **107**(B11), 2300, doi:10.1029/2000JB000050.

Daradich, A., Mitrovica, J., Matsuyama, I. & Perron, J., 2008. Equilibrium rotational stability and figure of mars, *Icarus,* **194,** 463–475.

Dziewonski, A.M. & Anderson, D.L., 1981. Preliminary reference earth model, *Phys. Earth planet. Inter.,* **25**(4), 297–356.

Forte, A.M. & Mitrovica, J.X., 1997. A resonance in the earth's obliquity and precession overthe past 20 myr driven by mantle convection, *Nature,* **390**(6661), 676–680.

Gold, T., 1955. Instability of the earth's axis of rotation, *Nature,* **175,** 526–529.

Goldreich, P. & Toomre, A., 1969. Some remarks on polar wandering, *J. geophys. Res.,* **74**(10), 2555–2567.

Gross, R., 2007. Earth rotation variations—long period, *Treatise Geophys.,* **3,** 239–294.

Kirschvink, J., Ripperdan, R. & Evans, D., 1997. Evidence for a large-scale reorganization of early cambrian continental masses by inertial interchange true polar wander, *Science,* **277**(5325), 541–545.

Latychev, K., Mitrovica, J., Tromp, J., Tamisiea, M., Komatitsch, D. & Christara, C., 2005. Glacial isostatic adjustment on 3-D earth models: a finite-volume formulation, *Geophys. J. Int.,* **161**(2), 421–444.

Lithgow-Bertelloni, C. & Silver, P.G., 1998. Dynamic topography, plate driving forces and the african superswell, *Nature,* **395,** 269–272.

Matsuyama, I., Mitrovica, J., Manga, M., Perron, J. & Richards, M., 2006. Rotational stability of dynamic planets with elastic lithospheres, *J. geophys. Res.,* **111,** E02003, doi:10.1029/2005JE002447.

Matsuyama, I., Mitrovica, J.X., Daradich, A. & Gomez, N., 2010. The rotational stability of a triaxial ice-age earth, *J. geophys. Res.,* **115,** B05401, doi:10.1029/2009JB006564.

Mitrovica, J., 1996. Haskell [1935] revisited, *J. geophys. Res.,* **101**(B1), 555–569.

Mitrovica, J. & Forte, A., 2004. A new inference of mantle viscosity based upon joint inversion of convection and glacial isostatic adjustment data, *Earth planet. Sci. Lett.,* **225**(1–2), 177–189.

Mitrovica, J., Wahr, J., Matsuyama, I. & Paulson, A., 2005. The rotational stability of an ice-age earth, *Geophys. J. Int.,* **161**(2), 491–506.

Munk, W.H. & MacDonald, G.J.F., 1960. The rotation of the earth: a geophysical discussion, Vol. 8, Cambridge University Press, New York, NY.

Nakada, M. & Lambeck, K., 1989. Late pleistocene and holocene sea-level change in the australian region and mantle rheology, *Geophys. J. Int.,* **96,** 497–517.

Nakiboglu, S., 1982. Hydrostatic theory of the earth and its mechanical implications, *Phys. Earth planet. Inter.,* **28,** 302–311.

Peltier, W., 1974. The impulse response of a maxwell earth, *Rev. Geophys. Space Phys.,* **12**(4), 649–669.

Peltier, W.R., 2004. Global glacial isostasy and the surface of the ice-age earth: the ice-5g (vm2) model and grace, *Annu. Rev. Earth planet. Sci.,* **32,** 111–149.

Ricard, Y., Spada, G. & Sabadini, R., 1993. Polar wandering of a dynamic earth, *Geophys. J. Int.,* **113,** 284–298.

Richards, M., Ricard, Y., Lithgow-Bertelloni, C., Spada, G. & Sabadini, R., 1997. An explanation for earth's long-term rotational stability, *Science,* **275,** 372–375.

Richards, M., Bunge, H.-P., Ricard, Y. & Baumgardner, J., 1999. Polar wandering in mantle convection models, *Geophys. Res. Lett.,* **26**(12), 1777–1780.

Sager, W. & Koppers, A.A.P., 2000. Late cretaceous polar wander of the pacific plate: evidence of a rapid true polar wander event, *Science,* **287,** 455–459.

Schaber, K., Bunge, H.-P., Schuberth, B.S.A., Malservisi, R. & Horbach, A., 2009. Stability of the rotation axis in high-resolution mantle circulation models: weak polar wander despite strong core heating, *Geochem. Geophys. Geosyst.,* **10,** Q11W04, doi:10.1029/2009GC002541.

Steinberger, B. & O'Connell, R., 1997. Changes of the earth's rotation axis owing to advection of mantle density heterogeneities, *Nature,* **387,** 169–173.

Steinberger, B. & Torsvik, T.H., 2008. Absolute plate motions and true polar wander in the absence of hotspot tracks, *Nature,* **452,** 620–623.

Thissen, C., Mitchell, R., Kirschvink, J., Evans, D., Montanari, A., Coccioni, R., Hinnov, L. & Tsai, V., 2010. True polar wobbles: cretaceous magnetostratigraphy provides continuous age-calibration and paleogeography, Abstract GP13A-0758 presented at *2010 Fall Meeting*, *AGU*.

Tromp, J. & Mitrovica, J.X., 1999. Surface loading of a viscoelastic earth—I. general theory, *Geophys. J. Int.,* **137,** 847–855.

Tsai, V. & Stevenson, D., 2007. Theoretical constraints on true polar wander, *J. geophys. Res.,* **112,** B05415, doi:10.1029/2005JB003923.

Willemann, R., 1984. Reorientation of planets with elastic lithospheres, *Icarus,* **60,** 701–709.

Wu, P., 1978. The response of a maxwell earth to applied surface mass loads, *MSc thesis*, Univ. Toronto.